

UvA-DARE (Digital Academic Repository)

Negative Thermal Expansion Design Strategies in a Diverse Series of Metal-Organic Frameworks

Burtch, N.C.; Baxter, S.J.; Heinen, J.; Bird, A.; Schneemann, A.; Dubbeldam, D.; Wilkinson, A.P.

DOI

[10.1002/adfm.201904669](https://doi.org/10.1002/adfm.201904669)

Publication date

2019

Document Version

Final published version

Published in

Advanced Functional Materials

License

Article 25fa Dutch Copyright Act

[Link to publication](#)

Citation for published version (APA):

Burtch, N. C., Baxter, S. J., Heinen, J., Bird, A., Schneemann, A., Dubbeldam, D., & Wilkinson, A. P. (2019). Negative Thermal Expansion Design Strategies in a Diverse Series of Metal-Organic Frameworks. *Advanced Functional Materials*, 29(48), [1904669]. <https://doi.org/10.1002/adfm.201904669>

General rights

It is not permitted to download or to forward/distribute the text or part of it without the consent of the author(s) and/or copyright holder(s), other than for strictly personal, individual use, unless the work is under an open content license (like Creative Commons).

Disclaimer/Complaints regulations

If you believe that digital publication of certain material infringes any of your rights or (privacy) interests, please let the Library know, stating your reasons. In case of a legitimate complaint, the Library will make the material inaccessible and/or remove it from the website. Please Ask the Library: <https://uba.uva.nl/en/contact>, or a letter to: Library of the University of Amsterdam, Secretariat, Singel 425, 1012 WP Amsterdam, The Netherlands. You will be contacted as soon as possible.

UvA-DARE is a service provided by the library of the University of Amsterdam (<https://dare.uva.nl>)

Negative Thermal Expansion Design Strategies in a Diverse Series of Metal–Organic Frameworks

Nicholas C. Burtch,* Samuel J. Baxter, Jurn Heinen, Ashley Bird, Andreas Schneemann, David Dubbeldam, and Angus P. Wilkinson

Negative thermal expansion materials are of interest for an array of composite material applications whereby they can compensate for the behavior of a positive thermal expansion matrix. In this work, various design strategies for systematically tuning the coefficient of thermal expansion in a diverse series of metal–organic frameworks (MOFs) are demonstrated. By independently varying the metal, ligand, topology, and guest environment of representative MOFs, a range of negative and positive thermal expansion behaviors are experimentally achieved. Insights into the origin of these behaviors are obtained through an analysis of synchrotron-radiation total scattering and diffraction experiments, as well as complementary molecular simulations. The implications of these findings on the prospects for MOFs as an emergent negative thermal expansion material class are also discussed.

1. Introduction

In condensed matter, an increase in temperature generally leads to an increase in volume. This phenomenon, known as positive thermal expansion (PTE), can cause significant stress or even catastrophic device failure in applications where materials are placed in confined environments. At material interfaces such as coatings or films, mismatches in thermal expansion properties can also lead to cracking and peeling. The development of tailored thermal expansion behaviors in materials would mitigate such problems and be of significant value for a variety of material design and engineering challenges.^[1]

While PTE is the norm in most materials, negative thermal expansion (NTE) has been observed in materials that include

oxides, fluorides, cyanides, polymers, and carbon nanotubes.^[2–6] A seminal discovery in this field was that ZrW_2O_8 ^[7] exhibits isotropic NTE ($\alpha_1 = (1/l)dl/dT \approx -9 \text{ ppm K}^{-1}$) over the 0.3–1050 K temperature range.^[8] Since this finding, a number of experimental and theoretical studies have shed light on the vibrational modes leading to this behavior and their implications for the design of further NTE materials.^[9,10] More recently, an increased interest has developed around tailoring thermal expansion via chemical modifications^[11] and through the use of phase transitions with magnetic, ferroelectric, charge-transfer and metal-insulator origins^[1] to achieve large-scale NTE. Outside of the materials science community,

however, the most ubiquitous NTE substance is water. Water has an increasing density with temperature over the 0–4 °C range due to the increased entropy resulting from the breaking of its tetrahedral hydrogen bonding network.^[12]

Zeolites and metal–organic frameworks (MOFs) are material classes that have been predicted to exhibit widespread NTE,^[13–17] due in part to their nanoporosity and flexible framework characteristics. MOFs, formed by the assembly of inorganic nodes and multitopic organic ligands,^[18,19] are particularly intriguing as NTE materials because of the greater design flexibility they afford relative to zeolites. The organic constituents in MOFs also enable a larger degree of structural flexibility^[20] which may further promote their potential for exhibiting large-scale NTE.


To date, isotropic NTE has been experimentally reported in a limited number of frameworks, including in the well-known HKUST-1 ($\text{Cu}_3(\text{BTC})_2$, BTC = 1,3,5-benzenetricarboxylate)^[21] and IRMOF-1 ($\text{Zn}_4\text{O}(\text{BDC})_3$, BDC = benzene-1,4-dicarboxylate)^[22] materials. Beyond computational studies on Zn_4O -based IRMOF variants,^[14,15] the systematic structural engineering of MOFs as an NTE material class has not been well explored. NTE in MOFs can also be accompanied by phase transitions, leading to discontinuities in their lattice parameters with temperature.^[23] Controlled thermal expansion in the absence of such phase transitions, however, is critical to the utility of NTE materials in most applications where the PTE matrix will change dimensions in a continuous fashion.

In this work, we demonstrate design strategies for tailoring thermal expansion in microporous MOFs. By independently varying the metal, ligand, topology, and guest species, we show

Dr. N. C. Burtch, A. Bird, Dr. A. Schneemann
Sandia National Laboratories
Livermore, CA 94550, USA
E-mail: nburtch@sandia.gov

S. J. Baxter, Prof. A. P. Wilkinson
School of Chemistry and Biochemistry
School of Materials Science and Engineering
Georgia Institute of Technology
Atlanta, GA 30332, USA

Dr. J. Heinen, Dr. D. Dubbeldam
Van't Hoff Institute for Molecular Sciences
University of Amsterdam
Science Park 904, 1098XH Amsterdam, The Netherlands

 The ORCID identification number(s) for the author(s) of this article can be found under <https://doi.org/10.1002/adfm.201904669>.

DOI: 10.1002/adfm.201904669

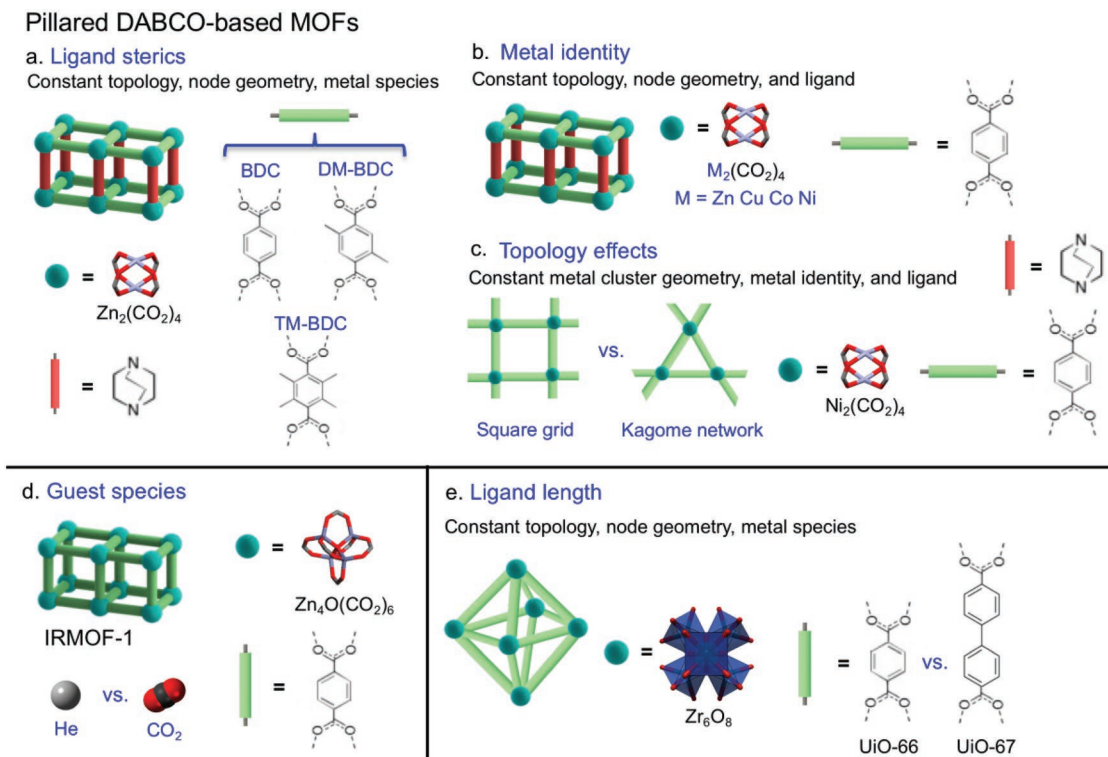


Figure 1. Overview of design strategies for thermal expansion control in nanoporous MOFs. a) Modifying the steric bulk of the ligand. b) Changing the identity of the metal in the inorganic cluster. c) Altering the framework topology. d) Varying the guest species. e) Altering the length of the ligand.

how MOF thermal expansion characteristics can be adjusted in the positive or negative direction. For promising MOF NTE material candidates possessing Zr_6O_8 -based secondary building units, we also analyze synchrotron-radiation pair distribution functions (PDFs) from total scattering experiments to investigate the impact of thermal history on their thermal expansion behavior. These insights, combined with molecular simulation analysis, are used to highlight the prospects and challenges towards the use of MOFs as an emergent NTE material class.

2. Results

We demonstrate various design strategies for achieving thermal expansion control in MOFs using the structures shown in **Figure 1**. M_2L_2 (DABCO) MOFs containing the 1,4-diazabicyclo[2,2,2]octane (DABCO) pillaring ligand (**Figure 1a–c**) enabled us to isolate the impact of the metal (M), topology, and steric bulk of functional groups on the linear dicarboxylate ligand (L) in the 2D M_2L_2 layered direction while keeping other structural features constant. IRMOF-1 (**Figure 1d**) is a prototypical MOF based on $Zn_4O(CO_2)_6$ clusters and benzene-1,4-dicarboxylate (BDC) ligands that has previously been shown to exhibit isotropic NTE.^[14,15,22] Here, we experimentally show that the identity of its incorporated guest species can be used as a strategy to tune the magnitude of its NTE. Lastly, the dependence of thermal expansion on the thermal history and length of the dicarboxylate ligand in Zr_6O_8 -based MOFs (**Figure 1e**) with minimal structural defects is presented.

The coefficients of thermal expansion in these systems were analyzed upon heating using variable-temperature synchrotron or laboratory powder diffraction experiments over a ≈ 10 – 100 °C temperature range. This temperature range is relevant to NTE applications where MOFs would be most suitable from a mechanical and thermal properties standpoint, such as fillers in organic matrices (e.g., polymers, epoxies, and resins), and also yielded near-linear behavior that enabled comparison of average coefficient of thermal expansion (CTE) values.

2.1. Ligand Steric Effects

Ligand design is an emerging strategy for altering the adsorption, chemical stability, and flexible framework dynamics of pillared MOFs.^[24–26] Applying this design principle towards isostructural DABCO-based MOFs possessing a $Zn_2(CO_2)_4$ cluster (**Figure 1a**), we observe an increase in the magnitude of NTE in the layered direction with decreasing steric hindrance on the dicarboxylate ligand. As shown in **Figure 2a**, by switching from BDC to its functionalized variants with an increasing number of methyl groups on the phenyl ring, we obtain average linear CTE values in the layered direction of $\alpha_l = -9.6(9)$ ppm K^{-1} (BDC), $-5.4(5)$ ppm K^{-1} (2,5-dimethyl-BDC, DM-BDC), and $4.2(2)$ ppm K^{-1} (2,3,5,6-tetramethyl-BDC, TM-BDC).

The experimental results are consistent with the computed average CTE values obtained from molecular dynamics simulations on the BDC, DM-BDC, and TM-BDC models of these structures ($\alpha_l = -6.7$, -6.4 , and 4.1 ppm K^{-1} , respectively). The primary structural differences among these variants arise

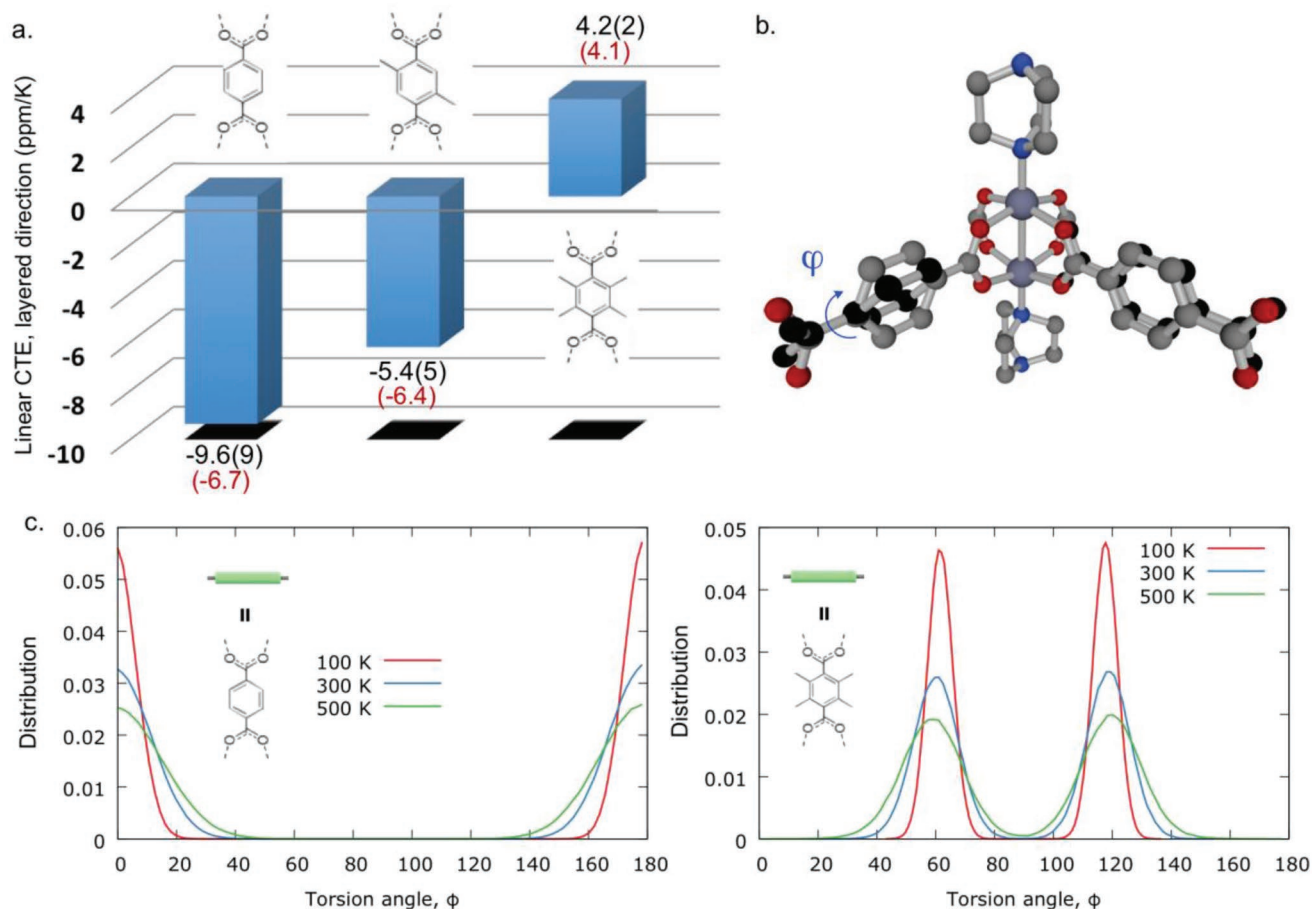


Figure 2. Thermal expansion and structural dynamics due to varying ligand steric effects. a) Average linear CTE from ≈ 10 to 100 °C in DABCO-based, $\text{Zn}_2(\text{CO}_2)_4$ MOFs with the square network motif and varying degrees of steric hindrance on their linear dicarboxylate ligand. Error estimates given as asymptotic standard error. Red values in parentheses were obtained from molecular dynamics simulations. b) Depiction of the dihedral vibrational mode of the aromatic ring (hydrogens and ligand substituents omitted for clarity) and c) corresponding normalized dihedral angle distribution profile for the BDC (left) and TM-BDC (right) structures as a function of temperature.

from the bulkiness of their functional groups and the torsion angle of their aromatic rings (Figure 2b). The importance of these structural differences on the resulting thermal expansion behavior was investigated using molecular simulation analysis.

While the temperature-dependent distribution of torsion angles (Figure 2c) remain Gaussian with temperature, the profiles of the bell-shaped curves in Zn-DMOF are wider than those observed in Zn-DMOF-TM for a given temperature, indicating an inhibition of the linker movement in Zn-DMOF-TM due to its methyl groups. We also observe that imposing the dihedral angle of the phenyl ring that is found in Zn-DMOF-TM on the Zn-DMOF structure, in the absence of any increased steric effects due to methyl groups, does not significantly inhibit its NTE (Figure S38, Supporting Information). However, as one gradually reduces the bulkiness of the methyl groups in the Zn-DMOF-TM framework, we observe an appreciable increase in the structure's NTE (Figures S39 and S40, Supporting Information), suggesting that the degree of steric repulsion due to the methyl groups in TM-BDC is a primary reason for the structure's observed PTE.

2.2. Topological and Metal Effects

DABCO-based MOFs possessing $\text{Ni}_2(\text{CO}_2)_4$ clusters with BDC in either a square or Kagome layered network motif (Figure 1c) were characterized to explore the impact of framework topology on their thermal expansion behavior. In the tetragonal framework, there is a single pore size in the layered direction with a 90° angle between each of the ligands at the metal cluster whereas the trigonal Kagome network contains two distinct pore openings. The Kagome network phase is kinetically favored over the square phase in the presence of Ni/BDC/DABCO mixtures^[27] and we obtained a two-phase sample containing both the square and Kagome motifs for analysis. Given the geometries of the two polymorphs, a low-energy interface that would enable intergrown crystals of the two phases seems unlikely, and we thus assume that there is no significant mechanical coupling whereby the thermal expansion of one phase would affect the other. The diffraction pattern exhibits well-distinguished Bragg peaks for the two phases (Figure S14, Supporting Information) and revealed NTE in the layered direction of both of these variants, with an increased

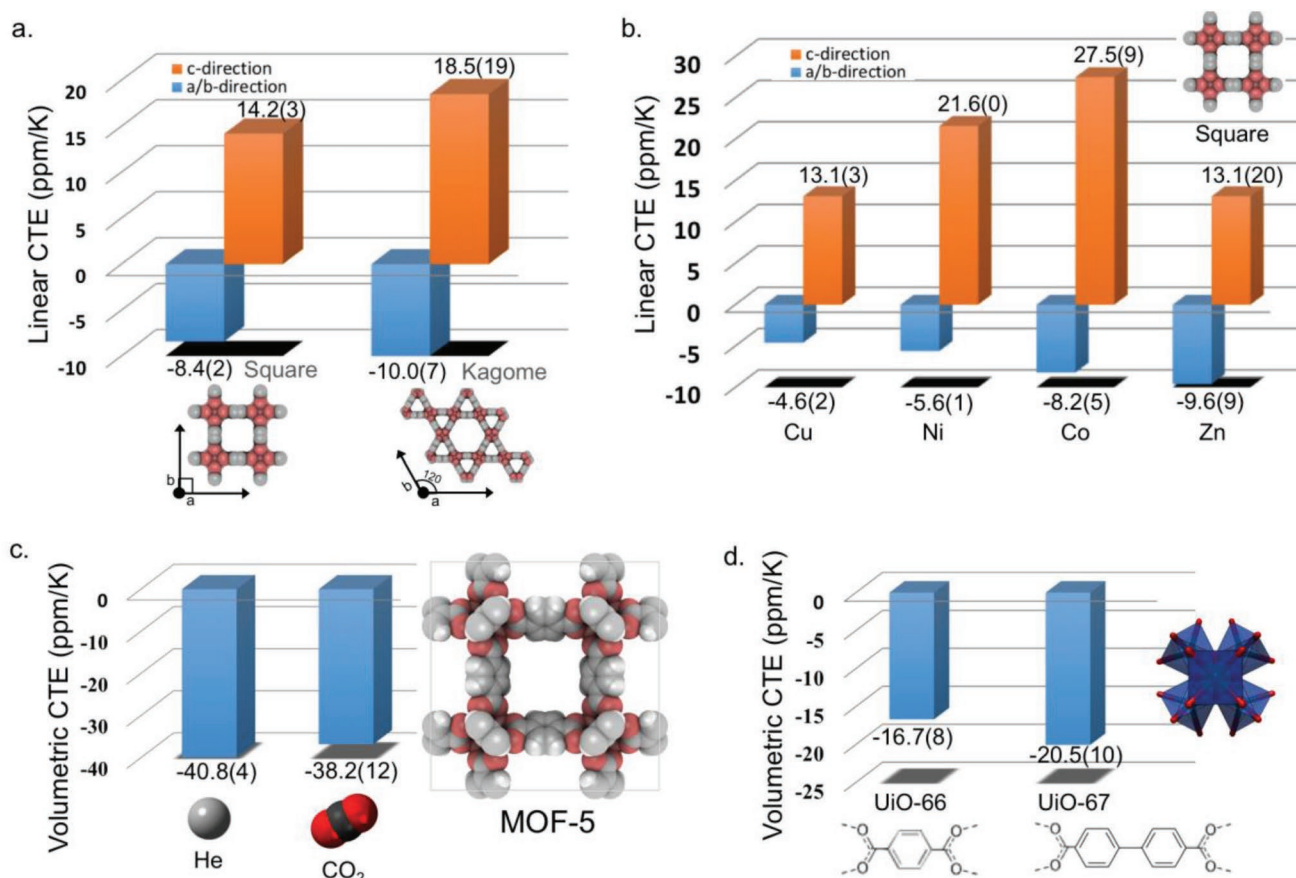


Figure 3. Thermal expansion behavior due to varying framework topology, metal, guest incorporation, and ligand length effects. a) Effect of topology in a DABCO-based Ni₂(CO₂)₄ two-phase square and Kagome network sample. b) Effect of the metal identity in DABCO-based square network frameworks with the inorganic cluster M₂(CO₂)₄ (M = Co, Ni, Cu, or Zn). c) Effect of guest species (helium or carbon dioxide) of IRMOF-1 at 1 atm gas pressure. d) Effect of ligand length in the Zr₆O₈-based UiO-66 and UiO-67 structures in the absence of significant node distortion.

magnitude of areal contraction upon heating for the Kagome material (Figure 3a) that is consistent with molecular modeling predictions from the square and Kagome layered analogs constructed using a Zn₂(CO₂)₄ cluster (Supporting Information).

The identity of the metal in the M₂(CO₂)₄ (M = Co, Ni, Cu, or Zn) cluster of DABCO-based MOFs possessing BDC as their square layered ligand affects the thermal expansion behavior in the manner shown in Figure 3b. Similar to the Zn₂(CO₂)₄-based structure, each of the variants exhibit NTE in their layered direction over the 10–100 °C temperature range. Relative to the other structures, the Zn-based material exhibits the highest magnitude of NTE. As the distance between adjacent paddlewheels in the *a*–*b* plane increases, as indicated by the room temperature lattice constants, the magnitude of NTE in the *a*–*b* plane also increases. This may be due to decreased steric interactions. In contrast, the PTE parallel to the *c*-axis generally decreases in moving from left to right across the periodic table, with the exception of zinc and copper where the experimentally determined CTEs are indistinguishable. The origin of this trend is unclear.

2.3. Guest Effects

The mechanism of isotropic NTE in the cubic IRMOF-1 material has been studied both experimentally^[22,28,29] and

computationally.^[14,15,30] Its NTE behavior is generally attributed to the ability of its octahedral Zn₄O(CO₂)₆ clusters and connecting ligands to tilt via transverse displacements to greater degrees upon increasing temperature. By varying the gas environment of IRMOF-1 from carbon dioxide to helium at 1 atm total pressure, a slight increase in the magnitude of its NTE from $\alpha_v = (1/V)dV/dT = -38.2(12)$ to $-40.8(4)$ ppm K⁻¹ is observed (Figure 3c). Such guest environment changes are relevant to the use of MOFs in selective sensing or adsorbent columns applications whereby a gas purge or temperature swing takes place after saturation with the target adsorbate. Carbon dioxide has stronger framework interactions than helium (which is often assumed non-adsorbing in porous materials) and thus carbon dioxide adsorbs to a higher equilibrium loading at a given temperature. One cannot delineate the framework's inherent NTE from guest loading effects, however, and the loading will be non-linear over temperature. Using a molecular model that is parameterized to capture the CO₂ adsorption behavior in MOF-5,^[31] over our experimental temperature range, we obtain approximate loadings of 4.5, 1.6, 0.8, 0.5, and 0.3 mol kg⁻¹ at 240, 270, 300, 330, and 360 K, respectively. This general behavior is consistent with the computationally predicted effects of host–guest interactions on the CTE of IRMOF-1 for the

more strongly interacting benzene, isopropanol, and propane molecules.^[30]

2.4. Ligand Length and Node Distortion Effects

The UiO-66 and UiO-67 MOFs possess Zr_6O_8 nodes that are 12-connected by BDC or biphenyl-4,4'-dicarboxylic acid (BPDC) in their defect-free forms.^[32] These materials are cubic and also exhibit exceptional chemical and thermal stability properties relative to many MOFs reported in the literature.^[33,34] As such, they are attractive candidates for NTE applications. Work by Chapman et al., however, reports that dehydroxylation of the UiO-66 structure's Zr_6O_8 node chemistry^[35] at temperatures above ≈ 120 – 130 °C can cause reversible structural distortions that result in a volume contraction in the material.^[36] These reversible distortions were not discernable from the average long-range structure observed from powder X-ray diffraction measurements but were clearly captured by PDF analyses of the total scattering data. Specifically, the disappearance of a single Zr...Zr atomic distance in the PDF at ≈ 3.5 Å, characteristic of the 12 equivalent Zr...Zr distances across the edges of a symmetric Zr_6 octahedron, and the simultaneous appearance of two additional peaks at ≈ 3.3 and 3.7 Å, corresponding to the Zr...Zr distances of a lower symmetry distorted octahedron, were observed.^[36] Given these possible Zr_6O_8 distortions, we analyzed both the local (node chemistry) and long-range (lattice parameter) changes in these materials via synchrotron total scattering and diffraction experiments.

The impact of thermal history on the thermal expansion behavior was studied through a comparison of the UiO-66 material's PDF after a heat pre-treatment of either 95 °C (UiO-66@95 °C) or 220 °C (UiO-66@220 °C) under helium for 2 h. For UiO-66@95 °C, we observe no significant splitting of the Zr...Zr PDF peak at ≈ 3.5 Å immediately after heat pre-treatment (Figure 4a) and, upon subsequent heating to ≈ 90 °C, we observe a CTE of $\alpha_V = -16.7(8)$ ppm K⁻¹. For UiO-66@220 °C, however,

significant node chemistry distortions result in a splitting of the ≈ 3.5 Å Zr...Zr peaks after heat pre-treatment, similar to the results reported by Chapman et al. (Figure 4b).^[36] Due to the contraction this distortion creates in the material, upon subsequent heating to ≈ 90 °C, UiO-66@220 °C exhibits a positive CTE of $\alpha_V = 14.8(24)$ ppm K⁻¹ as its Zr_6O_8 node relaxes (expands^[35]) back to its undistorted octahedron state. A comparison of the UiO-66@95 °C and UiO-67@95 °C structures shows an increase in magnitude of the volumetric CTE with the length of the organic ligand, from $\alpha_V = -16.7(8)$ to $-20.5(10)$ ppm K⁻¹ (Figure 3d), a trend that is qualitatively consistent with our molecular dynamics simulations reported in the Supporting Information on UiO-66 and UiO-67 ($\alpha_V = -16.6$ and -32.6 ppm K⁻¹, respectively).

3. Discussion

MOFs as an Emergent Negative Thermal Expansion Material Class: An ideal NTE material for composite material applications will have a large magnitude of NTE in order to minimize the amount of material needed to achieve the desired CTE reduction. Furthermore, in single-phase polycrystalline materials such as ceramics, anisotropic thermal expansion can be problematic and lead to internal microcracking and increased stress.^[37] Figure 5 provides a selection guide for isotropic NTE materials based on average CTE values reported for selected materials over various temperature ranges. The highest magnitude isotropic NTE materials include various Prussian blue analogs, metal cyanides, and metal fluorides. Depending on the target application, MOFs can provide advantages over traditional material classes that include an extended range over which NTE is exhibited, improved chemical, mechanical, and thermal stability properties^[33] and, due to their porosity, the exploitation of guest environment as a thermal expansion control strategy. On the other hand, while a lesser magnitude of NTE has been observed in material families that encompass zirconium vanadates, zirconium tungstates, and various

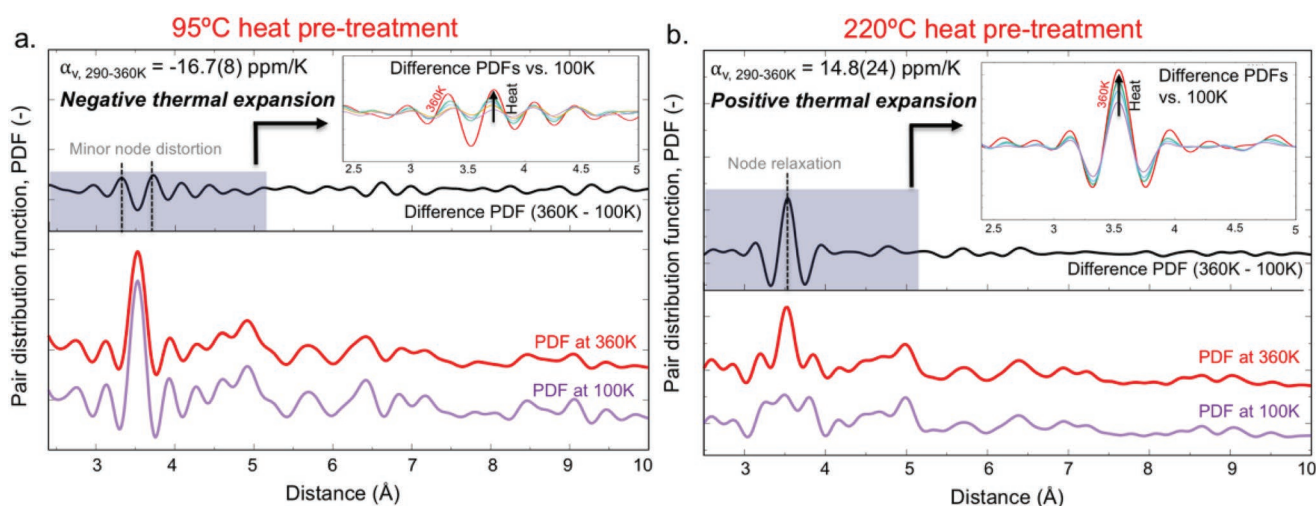


Figure 4. Effect of thermal history on UiO-66 Zr_6O_8 node geometry and its subsequent thermal expansion behavior upon heating. a) PDF changes after a 95 °C heat pre-treatment (UiO-66@95 °C), illustrating a scenario where no significant node distortion is initially present and NTE behavior is observed. b) PDF changes after a 220 °C (UiO-66@220 °C) heat pre-treatment, illustrating how a contraction due to node distortion being initially present in the structure can result in subsequent PTE.

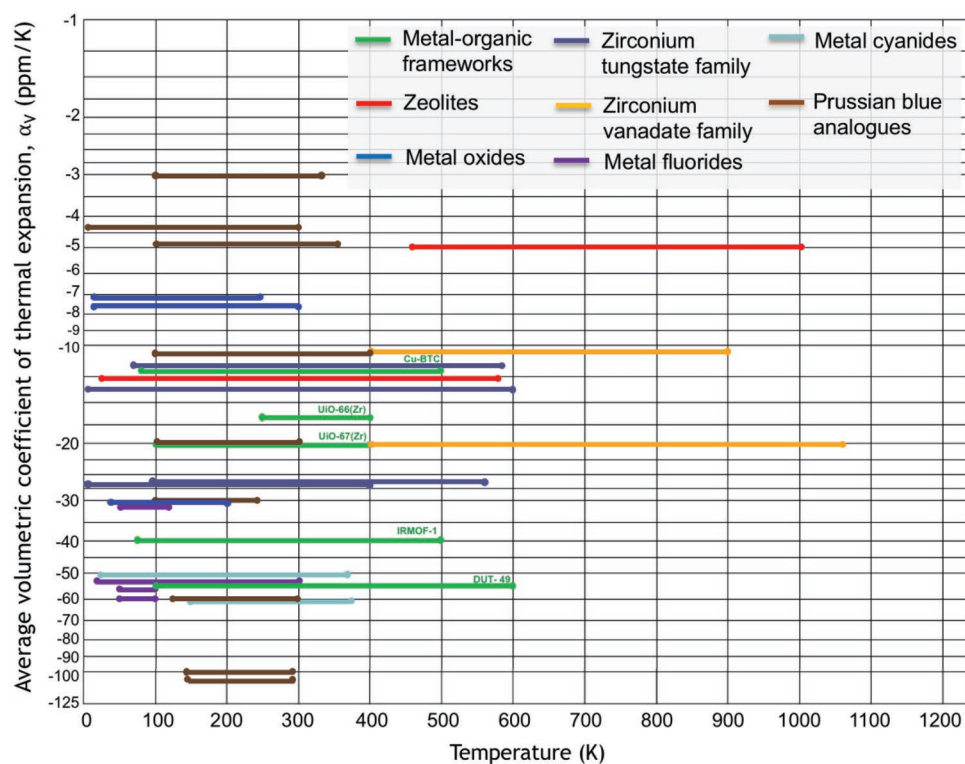


Figure 5. Selection guide for isotropic NTE crystalline materials. Average experimental volumetric CTE values reported for selected materials in various NTE material classes. Values for MOFs, zeolites, metal cyanides, Prussian blue analogues, and zirconium tungstate and vanadate families values are based on literature in Wells et al.^[9] DUT-49 value obtained from Krause et al.^[44] Selected metal fluoride values were taken from Hester et al.^[45] UiO-66(Zr) and UiO-67(Zr) values from this work are for the frameworks having undergone a 95 °C heat pre-treatment.

metal oxides, their chemical and thermal stability limits can far exceed those present in MOFs. Furthermore, one should consider the compatibility between the mechanical properties, such as bulk modulus and hardness, of the NTE material and its PTE matrix. In this regard, MOFs are likely most suitable for matrices that include foams, polymers, epoxies, and resins.^[20]

Unique attributes of MOFs that make them promising as an emergent NTE material class are their immense degree of structural tunability^[38] and the intriguing mechanical properties endowed by their hybrid organic–inorganic chemistry.^[39] The mechanical properties of MOFs bode well from an NTE standpoint. Given that $\alpha_v = (1/V)(\partial V/\partial T)_P$, thermodynamics and the Maxwell relations show that $\alpha_v = 1/B_T(\partial S/\partial V)_T$ (where $B_T = -V(\partial P/\partial V)_T$), suggesting that a high NTE material should also be relatively soft. In the context of other NTE materials, MOFs are promising, with B_T values from diamond anvil cell experiments and theoretical calculations in the range of low tens of GPa.^[20,39] While NTE is anticipated to be more pervasive in MOFs than in many other material classes, it is notably absent in prototypical materials such as the ZIF-8 ($Zn(MeIM)_2$, MeIM = 2-methylimidazole) framework,^[40] in which we observe PTE ($\alpha_v = 19.6(9)$ ppm K^{-1} , Figure S34, Supporting Information) that is consistent with previous computational predictions.^[41]

The node distortion behavior of Zr_6O_8 -based MOFs also suggests unique and exciting prospects for robustly compensating for the glass transition exhibited in amorphous and semicrystalline materials that progress from a relatively brittle to a more rubbery state upon heating. The glass transition in polymers

often leads to a relatively large ($\approx 3\text{--}5\times$ of the original value) increase in the CTE upon heating and can occur at temperatures similar to where node chemistry-induced contractions occur in Zr_6O_8 -based MOFs. We find that the temperature at which these contractions occur to be structure-dependent for UiO-66 and UiO-67, suggesting that design strategies for tailoring these contractions towards a desired temperature for targeted epoxies or polymer matrices can be employed.

Before becoming useful in composite material applications, studies into how the nanoscale (crystallographic) NTE found in MOFs translates to a CTE reduction at the macroscopic (bulk) scale must be performed. This requires thermomechanical analysis techniques for studying the change in length of a bulk specimen to capture important effects not evident from diffraction, such as changes to microstructure. Such characterizations have been performed on the well-studied ZrW_2O_8 material^[42] and have shed light on the importance of considerations that include particle dispersion, particle size, and appropriate surface interactions to promote adhesion between the NTE particle and its matrix. For MOFs, careful attention should also be placed on the effect of adsorbed guest species and whether confinement in the composite system gives rise to pressure-induced phase transitions.^[43]

4. Conclusions

This work adds to previous reports of NTE in MOFs, including those of anisotropic NTE attributed to hinge-like and

stretching-tilting mechanisms.^[46–48] Here, we have illustrated various design strategies for tailoring MOF thermal expansion behavior by varying their structural properties and guest environment. Through further characterization of the thousands of already synthesized MOFs, it is clear that additional design space in Figure 5 can be covered. A further design strategy that merits exploration is the controlled incorporation of defects in MOFs, such as what has been reported in the UiO-66(Hf) structure.^[49] More generally, a fundamental understanding of MOF thermal expansion is crucial to advancing their utility in a wide range of potential applications that include coated monoliths,^[50] microcantilever sensors, and electronic devices.^[51] In each of these scenarios, changes in temperature will arise, and a mismatch in the CTE of the MOF and its substrate material will produce residual stresses that can lead to cracking and peeling behavior or compromise the adhesion between the MOF and its interfaced layer.

5. Experimental Section

Sample synthesis and preparation details for all materials are given in the Supporting Information. To minimize the impact of structural defects on the thermal expansion behavior^[52] of UiO-66 and UiO-67, these materials were synthesized based on procedures reported by Lillerud et al.^[53,54] Nitrogen adsorption at 77 K was measured on each sample to confirm porosity characteristics before their storage under an argon environment until variable-temperature diffraction experiments were performed. Laboratory diffraction experiments were measured in a sealed quartz capillary using a nitrogen cyrostream for temperature control. Synchrotron-radiation diffraction and total scattering data were collected at beamline 17-BM-B and 11-ID-B of the Advanced Photon Source (APS) at Argonne National Laboratory using a Kapton capillary and a previously described sample cell environment.^[55] Lattice parameters were extracted via Pawley analysis with the GSAS-II software.^[56] Average linear CTE errors are reported with asymptotic standard errors from linear regression analysis. Classical simulations employed the RASPA molecular simulation software for adsorption and diffusion in flexible nanoporous materials.^[57] A description of the molecular simulation methodology and flexible force field models is included in the Supporting Information.

Supporting Information

Supporting Information is available from the Wiley Online Library or from the author.

Acknowledgements

N.C.B. acknowledges support from the Sandia National Laboratories Truman Fellowship Program, which is funded by the Laboratory Directed Research and Development (LDRD) Program. Sandia National Laboratories is a multimission laboratory managed and operated by National Technology and Engineering Solutions of Sandia, LLC., a wholly owned subsidiary of Honeywell International, Inc., for the U.S. Department of Energy's National Nuclear Security Administration under contract DE-NA0003525. Use of the Advanced Photon Source was supported by the U. S. Department of Energy, Office of Science, Office of Basic Energy Sciences, under Contract No. DE-AC02-06CH11357. Some images were created using the iRASPA software.^[58] This paper describes objective technical results and analysis. Any subjective views or opinions that might be expressed in the paper do not necessarily

represent the views of the U.S. Department of Energy or the United States Government.

Conflict of Interest

The authors declare no conflict of interest.

Keywords

metal–organic frameworks, negative thermal expansion, structural design strategies

Received: June 11, 2019
Revised: August 16, 2019
Published online: September 18, 2019

- [1] K. Takenaka, *Front. Chem.* **2018**, *6*, 267.
- [2] W. Miller, C. W. Smith, D. S. Mackenzie, K. E. Evans, *J. Mater. Sci.* **2009**, *44*, 5441.
- [3] C. Lind, *Materials* **2012**, *5*, 1125.
- [4] C. S. Coates, A. L. Goodwin, *Mater. Horiz.* **2018**.
- [5] D. J. Fisher, *Negative Thermal Expansion Materials*, Vol. 22, Materials Research Forum, Millersville, PA **2018**.
- [6] Z. Liu, K. Lin, Y. Ren, K. Kato, Y. Cao, J. Deng, J. Chen, X. Xing, *Chem. Commun.* **2019**, *55*, 4107.
- [7] J. Graham, A. D. Wadsley, J. H. Weymouth, L. S. Williams, *J. Am. Ceram. Soc.* **1959**, *42*, 570.
- [8] T. A. Mary, J. S. O. Evans, T. Vogt, A. W. Sleight, *Science* **1996**, *272*, 90.
- [9] M. T. Dove, H. Fang, *Rep. Prog. Phys.* **2016**, *79*, 066503.
- [10] R. Mittal, M. K. Gupta, S. L. Chaplot, *Prog. Mater. Sci.* **2018**, *92*, 360.
- [11] J. Chen, L. Hu, J. Deng, X. Xing, *Chem. Soc. Rev.* **2015**, *44*, 3522.
- [12] F. Cipcigan, V. Sokhan, G. Martyna, J. Crain, *Sci. Rep.* **2018**, *8*, 1718.
- [13] P. Lightfoot, D. A. Woodcock, M. J. Maple, L. A. Villaescusa, P. A. Wright, *J. Mater. Chem.* **2001**, *11*, 212.
- [14] D. Dubbeldam, K. S. Walton, D. E. Ellis, R. Q. Snurr, *Angew. Chem., Int. Ed.* **2007**, *46*, 4496.
- [15] S. S. Han, W. A. Goddard, *J. Phys. Chem. C* **2007**, *111*, 15185.
- [16] F. X. Coudert, J. D. Evans, *Coord. Chem. Rev.* **2019**, *388*, 48.
- [17] A. F. Sapnik, H. S. Geddes, E. M. Reynolds, H. H. M. Yeung, A. L. Goodwin, *Chem. Commun.* **2018**, *54*, 9651.
- [18] O. M. Yaghi, M. O'Keeffe, N. W. Ockwig, H. K. Chae, M. Eddaoudi, J. Kim, *Nature* **2003**, *423*, 705.
- [19] S. Kitagawa, R. Kitaura, S. Noro, *Angew. Chem., Int. Ed.* **2004**, *43*, 2334.
- [20] J. C. Tan, A. K. Cheetham, *Chem. Soc. Rev.* **2011**, *40*, 1059.
- [21] Y. Wu, A. Kobayashi, G. Halder, V. Peterson, K. W. Chapman, N. Lock, P. Southon, C. Kepert, *Angew. Chem.* **2008**, *120*, 9061.
- [22] W. Zhou, H. Wu, T. Yildirim, J. R. Simpson, A. R. H. Walker, *Phys. Rev. B* **2008**, *78*, 054114.
- [23] S. Henke, A. Schneemann, R. A. Fischer, *Adv. Funct. Mater.* **2013**, *23*, 5990.
- [24] N. C. Burtch, K. S. Walton, *Acc. Chem. Res.* **2015**, *48*, 2850.
- [25] W. Lu, Z. Wei, Z.-Y. Gu, T.-F. Liu, J. Park, J. Park, J. Tian, M. Zhang, Q. Zhang, T. Gentle III, M. Bosch, H.-C. Zhou, *Chem. Soc. Rev.* **2014**, *43*, 5561.
- [26] S. Henke, A. Schneemann, A. Wütscher, R. A. Fischer, *J. Am. Chem. Soc.* **2012**, *134*, 9464.

- [27] Y. Wu, S. Henke, G. Kieslich, I. Schwedler, M. Yang, D. A. X. Fraser, D. O'Hare, *Angew. Chem., Int. Ed.* **2016**, *55*, 14081.
- [28] N. Lock, M. Christensen, C. J. Kepert, B. B. Iversen, *Chem. Commun.* **2013**, *49*, 789.
- [29] N. Lock, Y. Wu, M. Christensen, L. J. Cameron, V. K. Peterson, A. J. Bridgeman, C. J. Kepert, B. B. Iversen, *J. Phys. Chem. C* **2010**, *114*, 16181.
- [30] S. R. G. Balestra, R. Bueno-Perez, S. Hamad, D. Dubbeldam, A. R. Ruiz-Salvador, S. Calero, *Chem. Mater.* **2016**, *28*, 8296.
- [31] K. S. Walton, A. R. Millward, D. Dubbeldam, H. Frost, J. J. Low, O. M. Yaghi, R. Q. Snurr, *J. Am. Chem. Soc.* **2008**, *130*, 406.
- [32] J. H. Cavka, S. Jakobsen, U. Olsbye, N. Guillou, C. Lamberti, S. Bordiga, K. P. Lillerud, *J. Am. Chem. Soc.* **2008**, *130*, 13850.
- [33] A. J. Howarth, Y. Liu, P. Li, Z. Li, T. C. Wang, J. T. Hupp, O. K. Farha, *Nat. Rev. Mater.* **2016**, *1*, 15018.
- [34] N. C. Burtch, H. Jasuja, K. S. Walton, *Chem. Rev.* **2014**, *114*, 10575.
- [35] L. Valenzano, B. Civaleri, S. Chavan, S. Bordiga, M. H. Nilsen, S. Jakobsen, K. P. Lillerud, C. Lamberti, *Chem. Mater.* **2011**, *23*, 1700.
- [36] A. E. Platero-Prats, A. Mavrandonakis, L. C. Gallington, Y. Liu, J. T. Hupp, O. K. Farha, C. J. Cramer, K. W. Chapman, *J. Am. Chem. Soc.* **2016**, *138*, 4178.
- [37] R. Roy, D. K. Agrawal, H. a McKinstry, *Annu. Rev. Mater. Sci.* **1989**, *19*, 59.
- [38] H.-C. Zhou, J. R. Long, O. M. Yaghi, *Chem. Rev.* **2012**, *112*, 673.
- [39] N. C. Burtch, J. Heinen, T. D. Bennett, D. Dubbeldam, M. D. Allendorf, *Adv. Mater.* **2018**, *30*, 1704124.
- [40] K. S. Park, Z. Ni, A. P. Côté, J. Y. Choi, R. Huang, F. J. Uribe-Romo, H. K. Chae, M. O'Keeffe, O. M. Yaghi, *Proc. Natl. Acad. Sci. USA* **2006**, *103*, 10186.
- [41] L. Bouéssel, A. U. Ortiz, A. Boutin, F. X. Coudert, *APL Mater.* **2014**, *2*, 124110.
- [42] C. Lind, M. R. Coleman, L. C. Kozy, G. R. Sharma, *Physica Status Solidi (b)* **2011**, *248*, 123.
- [43] A. Schneemann, V. Bon, I. Schwedler, I. Senkovska, S. Kaskel, R. A. Fischer, *Chem. Soc. Rev.* **2014**, *43*, 6062.
- [44] S. Krause, V. Bon, I. Senkovska, U. Stoeck, D. Wallacher, D. M. Töbrens, S. Zander, R. S. Pillai, G. Maurin, F. X. Coudert, S. Kaskel, *Nature* **2016**, *532*, 348.
- [45] B. R. Hester, J. C. Hancock, S. H. Lapidus, A. P. Wilkinson, *Chem. Mater.* **2017**, *29*, 823.
- [46] L. Zhang, X. Kuang, X. Wu, W. Yang, C. Lu, *Dalton Trans.* **2014**, *43*, 7146.
- [47] P. Lama, R. K. Das, V. J. Smith, L. J. Barbour, *Chem. Commun.* **2014**, *50*, 6464.
- [48] L. D. Devries, P. M. Barron, E. P. Hurley, C. Hu, W. Choe, *J. Am. Chem. Soc.* **2011**, *133*, 14848.
- [49] M. J. Cliffe, J. A. Hill, C. A. Murray, F.-X. Coudert, A. L. Goodwin, *Phys. Chem. Chem. Phys.* **2015**, *17*, 11586.
- [50] L. A. Darunte, Y. Terada, C. R. Murdock, K. S. Walton, D. S. Sholl, C. W. Jones, *ACS Appl. Mater. Interfaces* **2017**, *9*, 17042.
- [51] I. Stassen, N. Burtch, A. Talin, P. Falcaro, M. Allendorf, R. Ameloot, *Chem. Soc. Rev.* **2017**, *46*, 3185.
- [52] A. L. Goodwin, M. Calleja, M. J. Conterio, M. T. Dove, J. S. O. Evans, D. A. Keen, L. Peters, M. G. Tucker, *Science* **2008**, *319*, 794.
- [53] G. C. Shearer, S. Chavan, S. Bordiga, S. Svelle, U. Olsbye, K. P. Lillerud, *Chem. Mater.* **2016**, *28*, 3749.
- [54] S. Øien, D. Wragg, H. Reinsch, S. Svelle, S. Bordiga, C. Lamberti, K. P. Lillerud, *Cryst. Growth Des.* **2014**, *14*, 5370.
- [55] P. J. Chupas, K. W. Chapman, C. Kurtz, J. C. Hanson, P. L. Lee, C. P. Grey, *J. Appl. Crystallogr.* **2008**, *41*, 822.
- [56] B. H. Toby, R. B. Von Dreele, *J. Appl. Crystallogr.* **2013**, *46*, 544.
- [57] D. Dubbeldam, S. Calero, D. E. Ellis, R. Q. Snurr, *Mol. Simul.* **2016**, *42*, 81.
- [58] D. Dubbeldam, S. Calero, T. J. H. Vlugt, *Mol. Simul.* **2018**, *7022*, 1.